Semiclassical Dynamics and Quantum Control in Condensed Phases: Application to I_2 in a Solid Argon Matrix

Jianwei Che, Michael Messina,* and Kent R. Wilson

Department of Chemistry and Biochemistry, University of California, San Diego, La Jolla, California 92093-0339

V. A. Apkarian, Z. Li, C. C. Martens, and R. Zadoyan

Department of Chemistry, University of California, Irvine, California 92717-2025

YiJing Yan

Department of Chemistry, Hong Kong University of Science and Technology, Kowloon, Hong Kong

Received: October 16, 1995; In Final Form: January 15, 1996[⊗]

A novel scheme is developed which allows for the combination of classical sampling techniques and quantum wave packet dynamics to study both the inhomogeneous structural effects and the homogeneous dynamical effects in condensed phases. We utilize this methodology to theoretically investigate quantum control of the vibrational dynamics of a chromophore embedded in a condensed-phase environment. We consider control of the vibrational dynamics on an excited electronic state of I_2 that has been embedded in a low-temperature argon matrix, to compare with the work of Apkarian, Zadoyan, Martens, and co-workers. The high dimensionality of such systems precludes the possibility of an exact quantum treatment. To overcome this difficulty we take a semiclassical approach using Gaussian wave packet dynamics in the weak response regime. We compare the numerical simulation with experimental pump−probe measurements of Zadoyan and Apkarian, and we find reasonable agreement over the short time interval within which we will attempt to control the vibrational dynamics of the system in this work. Our calculations predict that coherent quantum control is indeed possible in this condensed-phase system at sufficiently short times and provide a measure of how its effectiveness falls off with time in comparison with the parallel gas-phase case. Finally, we summarize some of the conclusions about quantum control which may be drawn from this work and our other theoretical studies of quantum control in condensed-phase environments.

I. Introduction

Quantum control of molecular dynamics, defined as the use of tailored light pulses to optimally drive a quantum system to a desired final outcome, has now been realized both theoretically and experimentally for several types of chemically interesting systems.[1−8] For the most part, these systems have been of small dimensionality and restricted to the gas phase. (For an example of an approximate treatment of quantum control in a larger system see the work of Rice and Zhao.[9]) For these gas-phase systems there has been a rich variety of chemically interesting objectives of quantum control. These include selective bond breaking,[10,11] control of asymptotic translational,[12−14] vibrational,[15−21] rotational,[22] and stereochemical internal states[23,24] and electronic state populations,[25,26] and the rational tuning of branching ratios in reactions with physically or chemically distinct products.[27−31]

We have recently considered control of a different sort that is more transient in its nature.[8,32−41] This control paradigm is to determine the light field that optimally guides an evolving quantum system to a predetermined target state at a particular target time. Using this paradigm for quantum control we were able to demonstrate both theoretically[32−41] and experimentally[42,43] that control of the dynamics of an evolving quantum system is possible and that the degree of control intimately depends on the tailoring of the controlling light field and not just on its intensity versus frequency, $|E(\omega)|^2$, and its intensity versus time, $|E(t)|^2$. Control in this case is truly coherent. Within this paradigm for quantum control, we were able to theoretically and experimentally demonstrate coherent control for small gas-phase quantum systems. In this present paper, we turn to the more challenging problem of control in the condensed phase.

One would suspect that the ability to control the dynamics of an evolving quantum system in the condensed phase is hindered by two major obstacles, the first being an inhomogeneous effect and the second being homogeneous. In a condensed-phase system at a nonzero temperature there are a multitude of initial states of the system that are populated, and an optimal field that is specially tailored to control the dynamics of any particular initial state may be inappropriate to control the dynamics of another initial state of the system; this is an inhomogeneous effect. In a condensed-phase system containing many degrees of freedom, even for a single initial condition, the ability to control the dynamics of a subset of the system can be hindered by the coupling to other degrees of freedom, e.g., the transfer of energy among the degrees of freedom in the system; this is a homogeneous effect. Previously we have implemented a nearly classical approximation to quantum control and studied the controllability of the dynamics of I_2 in a rare-gas supercritical fluid environment at liquid density and room temperature.[8,36,37] This work revealed that control in a liquid density environment is limited, in that to succeed it must be done very quickly. A drawback of studying this room temperature supercritical liquid system is that both inhomoge-

[⊗] Abstract published in *Advance ACS Abstracts,* April 1, 1996.

S0022-3654(95)03059-0 CCC: $12.00

neous and homogeneous effects are involved simultaneously and their effects on controllability are entangled. An easy way to minimize the inhomogeneous effects is to consider a crystalline solid condensed-phase system at a very low temperature. In this way, the variety of initial conditions of the system will be minimized.

Fortunately, a recent set of experiments together with theoretical interpretation have recently been done on just such a system: I_2 embedded in solid rare-gas matrices at low temperatures. In these experiments,[44−46] I_2 is excited from the ground X state to the dissociative A state. In the gas phase, at the photon energy considered here, the I_2 would dissociate with unit quantum yield. The dynamics of the I_2 was then probed by using a second pulse to further excite the I_2 on the A state to the higher lying β ion pair state, and the laser-induced fluorescence (LIF) was collected as a function of pump−probe delay to yield the experimental signal. Two main results of this work are (i) the unambiguous demonstration of the caging effect by the surrounding rare-gas solid on the dissociating I_2, i.e., the I_2 does not dissociate in the condensed-phase environment as it would have in the gas phase, and (ii) the very long coherence of the wave packet motion on the A state. Peaks were observed in the LIF signal as long as 5 ps after the initial excitation pulse, which demonstrates that the I_2 wave packet can be localized over this long time scale. These two important results are further confirmed by classical simulation of the dynamics,[44−46] which was able to reasonably reproduce the results of the experiment. This system is thus an appealing candidate to study quantum control in the condensed phase.

Using our paradigm of quantum control described above, we will numerically study the controllability of the wave packet dynamics of I_2 that has been embedded in solid argon. We attempt to control a small part of the entire system, the dynamics of the I_2 molecule, while leaving the surrounding argon solid uncontrolled. Thus, we need a methodology whereby quantum control is only specified for a reduced dimensionality of the composite system. We are then led to the reduced density matrix, defined as the total density matrix for the entire system, $I_2 + Ar_n$, traced over the argon degrees of freedom. Our objective is thus to control the reduced density matrix of the composite system with an optimal specially tailored light field. Since quantum control is a quantum mechanical construct, we need to be able to solve the time-dependent Schrödinger equation (TDSE) in order to determine the optimal control fields. Since an exact solution of the TDSE is impossible for a condensed-phase system, we wish to use a reasonable set of approximations, allowing for as accurate a solution of the TDSE as is practical. In previous work we have shown that semiclassical propagation of wavepackets using Gaussian wave packet (GWP) dynamics[47] can lead to a practical and accurate short time solution of the quantum control equations.[39]

This paper is organized as follows: in section II we present a series of approximations that allow an efficient approximate semiclassical solution of the TDSE for a condensed phase system, in section III we derive equations to arrive at the optimal fields that drive the reduced density matrix of the system to a desired target state, in section IV we present the details of the numerical simulation, and in section V we present our conclusions.

II. Semiclassical Approach to Structure and Dynamics in the Condensed Phase

We consider a system consisting of many degrees of freedom, some of which are more interesting than others. There are many systems that enable such a discrimination among their degrees of freedom. For instance, for I_2 in an argon bath, the internal degrees of freedom of the I_2 molecule can be segregated from the rest of the system. To clarify the following discussion, we call the more interesting part of the condensed-phase system the primary system (the part of the system which will ultimately be controlled), the rest of the system the bath, and the composite of the primary system and the bath the supersystem. We label the degrees of freedom of the primary system by a collective coordinate $\mathbf{Q}$ that indicates either a single degree of freedom or a small collection of degrees of freedom, and we label the bath by the set of coordinates $\mathbf{x}$. The complete set of coordinates of the supersystem will be denoted by $\mathbf{q} \equiv (\mathbf{Q}, \mathbf{x})$. For simplicity, we will also assume that the supersystem has two electronic states, a ground state $|g\rangle$ and an excited state $|e\rangle$, radiatively coupled by an external light field, $\epsilon(t)$, although that can be generalized. The coupled matter-field Hamiltonian is

$$H(t) = H_m(\mathbf{Q}, \mathbf{x}) - D(\mathbf{Q}) \cdot \epsilon(t) \tag{1}$$

within the dipole approximation. Here H_m is the material, field-free Hamiltonian,

$$H_m = H_{sys}(\mathbf{Q}) + H_{bath}(\mathbf{x}) + V_c(\mathbf{Q}, \mathbf{x}) \tag{2}$$

where $H_{sys}(\mathbf{Q})$ is the primary system Hamiltonian, $H_{bath}(\mathbf{x})$ is the bath Hamiltonian, and $V_c(\mathbf{Q}, \mathbf{x})$ is the coupling between the bath and the primary system. Under the assumption that the bath is not directly coupled to the light field, we have

$$H_{sys}(\mathbf{Q}) = H_g(\mathbf{Q})|g\rangle\langle g| + [H_e(\mathbf{Q}) + \hbar\omega_{eg}]|e\rangle\langle e| \tag{3}$$

In above equation, ω_{eg} is the electronic transition frequency, which is assumed to be much larger than the vibrational energy spacings in both the ground and excited electronic state manifolds. In eq 1, $D(\mathbf{Q})$ is the transition dipole operator which we assume is independent of the bath coordinates.

Since we are considering a dynamic process whereby the light field in eq 1 drives the dynamics of the supersystem, the full dynamical evolution of the supersystem under the Hamiltonian in eq 1 must be considered. In this paper we represent the dynamics of the supersystem in Liouville space[48] whereby the density operator $\rho(t)$ is used to describe the temporal evolution. Since more interest usually lies in the time evolution of the primary system, a useful construct for considering this smaller subspace of the larger quantum system is the reduced density matrix, $\rho^R(t)$, defined as

$$\rho^{\mathrm{R}}(t) \equiv \mathrm{Tr}_{\mathrm{bath}}[\rho(t)] \tag{4}$$

The symbol $\mathrm{Tr}_{\mathrm{bath}}[...]$ denotes the trace over all the degrees of freedom of the bath. The Liouville space formalism has the advantages of straightforwardly treating the mixed states of the supersystem that arise at nonzero temperature and of allowing for a smooth transition between a hierarchy of approximations to the dynamics that can include classical, semiclassical, and finally exact quantum dynamics. This latter advantage of the Liouville space formulation is exceedingly important in this work, where we consider a condensed-phase system that excludes the possibility of an exact quantum treatment.

In a condensed-phase system, there are two main challenges to the evaluation of the time-dependent reduced density matrix. The first is the description of the initial quantum density matrix $\rho_g(t_0)$ in the condensed phase, i.e., the initial density matrix containing the inhomogeneous effect of the environment, and the second is the time propagation of the density matrix of the supersystem. The dynamical effect of the bath on the system

(i.e., homogeneous contributions, such as energy relaxation and pure dephasing) can only be analyzed by examining the time evolution of the reduced density matrix. This can, in principle, be performed within either a reduced or full dynamical propagation scheme. In reduced dynamical propagation, the dynamical effect of the bath on the system is introduced phenomenologically by a fluctuating random force and corresponding dissipation, while in full dynamical propagation the effect of the bath is considered explicitly and microscopically through the complete density matrix. In the latter case, the reduced matrix is obtained from tracing the full density matrix of the system over the bath degrees of freedom. In order to gain microscopic insight into the effect of the bath on the dynamics, we will propagate the full density matrix. This is an impossible task to perform exactly for a condensed-phase system, and thus it is critical to develop an approximate methodology. Unfortunately, there are a very small set of universally applicable techniques for solving the Liouville−Von Neumann equation. On the other hand, a wide and varied set of tools are available for the exact and approximate solution of the time-dependent Schrödinger equation (TDSE). In order to make use of these existing techniques, the initial density matrix $\rho(t_0)$ can be represented in a way that is consistent with Schrödinger space wavefunction propagation while properly representing the quantum distribution of the supersystem at thermal equilibrium. We thus compose the time evolved density matrix from an appropriate weighted average over a set of initially pure Schrödinger states.

In the following we will outline a method for evolving the full-density matrix of the system. This approximation has two components, the first being an approximation to the nonzero temperature averaging over the pure initial states of the condensed-phase system and the second being an approximation to the quantum dynamics of each initial pure state. Thus we present a rational series of approximations that allow for a tractable calculation of the reduced density matrix in a large quantum system.

In a condensed-phase system consisting of 10^{23} degrees of freedom, the composition of the density matrix of the supersystem from a Boltzmann weighted average over initial pure states is impossible to perform exactly, as the multitude of initial states that are populated at a non-zero temperature makes the Boltzmann weighted averaging over these states intractable. Therefore we will approximate the density matrix at any time $t \geq t_0$ as follows. (In order to simplify the notation, we will abbreviate the phase space point as $\mathbf{\Gamma} = (\mathbf{p}, \mathbf{q})$ and the phase space integration as $\int d\mathbf{\Gamma} = \int\int d\mathbf{p}\, d\mathbf{q}$.) The density matrix at time t is written as,

$$\rho(t) = \int d\mathbf{\Gamma}_0\, \rho_{cl}(\mathbf{\Gamma}_0; T')\rho_D(t; \mathbf{\Gamma}_0) \tag{5}$$

In eq 5, $\rho_{cl}(\mathbf{\Gamma}_0; T')$ is the classical phase space distribution function at an effective temperature T' which will be specified later. Physically, this function represents the thermal smearing of the system. The dynamical component $\rho_D(t; \mathbf{\Gamma}_0)$ of the density matrix $\rho(t)$, which parametrically depends on the classical phase space sampling point $\mathbf{\Gamma}_0$, is propagated from the initial $\rho_D(t_0; \mathbf{\Gamma}_0)$ to account for all the dynamics. Physically, the parameters $\mathbf{\Gamma}_0 = (\mathbf{p}_0, \mathbf{q}_0)$ can be the expectation values of momenta and coordinates in a system with the initial $\rho_D(t_0)$. Equation 5 formally separates the inhomogeneous (ensemble) and the homogeneous (dynamical) contributions as represented by ρ_{cl} and ρ_D, respectively. Furthermore, the initial $\rho_D(t_0; \mathbf{\Gamma}_0)$ can be chosen as a quantum correction to the classical distribution. The form of the dynamical component of the density matrix in eq 5, ρ_D, is flexible and depends on how the quantum dynamics of the system is to be calculated. This allows for a hierarchy of approximation schemes, such as exact quantum, semiclassical, and completely classical, for the dynamics. The nature of ρ_D sets the effective temperature T' and further defines the classical (inhomogeneous) ensemble contribution, $\rho_{cl}(\mathbf{\Gamma}_0)$. In the following paragraphs, we discuss some limiting cases and practical approaches for choosing the effective classical phase space distribution, ρ_{cl}, the initial dynamical component of the density matrix, $\rho_D(t_0)$, and appropriate methods for the time evolution of $\rho_D(t)$.

In the case that a direct propagation of the quantum density matrix is possible,[49,50] the dynamical component of the density matrix ρ_D is identical to the exact density matrix, i.e., $\rho_D(t) = \rho(t)$, and the effective classical distribution $\rho_{cl}(\mathbf{\Gamma}_0; T')$ is a Dirac δ function in $\mathbf{\Gamma}_0 = (\mathbf{p}_0, \mathbf{q}_0)$. This distribution is associated with an effective temperature $T' = 0$, since all the quantum effects of the nonzero temperature have been taken care of in the quantum distribution function $\rho_D(t_0) = \rho(t_0)$. Another interesting limit is when the dynamics is calculated completely classically. In this case ρ_D takes the form $\rho_D(\mathbf{\Gamma}, t; \mathbf{\Gamma}_0) = \delta(\mathbf{\Gamma} - \mathbf{\Gamma}_t)$, where $\mathbf{\Gamma}_t = (\mathbf{p}_t, \mathbf{q}_t)$ is the classical trajectory of the supersystem with the initial condition $\mathbf{\Gamma}_0 = (\mathbf{p}_0, \mathbf{q}_0)$ at time $t = t_0$. Therefore the corresponding classical distribution becomes the exact density matrix at the initial time, which in the Wigner phase space representation is given as

$$\rho_{cl}(\mathbf{\Gamma}_0; T') = \rho_w(\mathbf{\Gamma}_0, t_0) \tag{6}$$

In this case, the classical sampling temperature has to be adjusted, so that the classical distribution matches the quantum equilibrium distribution function $\rho_w(\mathbf{\Gamma}, t_0 \rightarrow -\infty)$ at the true temperature T. The mapping from the quantum Wigner phase space representation to a classical phase space representation can be carried out exactly in an ensemble of harmonic oscillators with a single frequency ω. In this case, the exact density matrix at the initial time in the Wigner phase space representation is given by

$$\rho_w(p,q,\beta) = \frac{1}{2\pi\hbar(\bar{n} + 1/2)} \exp\left[-\frac{q^2}{(2\hbar/m\omega)(\bar{n} + 1/2)} - \frac{p^2}{2m\hbar\omega(\bar{n} + 1/2)}\right] \tag{7}$$

where $\bar{n}$ is the Boson occupation number with $\bar{n} = (e^{\beta\hbar\omega} - 1)^{-1}$, ω is the frequency of the oscillator, and m is its mass. Using eq 6, we get the classical sampling temperature T_c' via the following relation with the true temperature[51]

$$T_c' = \frac{\hbar\omega}{k_B}\left(\bar{n} + \frac{1}{2}\right) \equiv \frac{\hbar\omega}{2k_B} \coth\left(\frac{\hbar\omega}{2k_B T}\right) \tag{8}$$

Now, we consider an approximation to the quantum dynamical evolution of the Schrödinger wavefunction for each phase space ensemble $(\mathbf{\Gamma}_0)$. This approximation will require that $\rho_D(t_0; \mathbf{\Gamma}_0)$ be in a pure state for each phase space ensemble at the initial time t_0, and consequently $\rho_D(t; \mathbf{\Gamma}_0)$ will then remain a pure state. That is

$$\rho_D(t; \mathbf{\Gamma}_0) = |\Psi(t; \mathbf{\Gamma}_0)\rangle\langle\Psi(t; \mathbf{\Gamma}_0)| \tag{9}$$

for all time $t \geq t_0$. As we mentioned previously, once the form of $\rho_D(t; \mathbf{\Gamma}_0)$ is chosen, in principle, the form of $\rho_{cl}(\mathbf{\Gamma}_0; T')$ is then determined. However, the exact evaluation of ρ_{cl} would require the complete knowledge of the exact quantum thermal

equilibrium density matrix, which is a very difficult problem itself for systems of large degrees of freedom.

In the following, we propose a semiclassical approach whereby $\rho_{cl}(\mathbf{\Gamma}_0; T')$ can be approximately constructed by an effective classical Boltzmann distribution. This is done by choosing the initial $\rho_D(t_0) = |\Psi(t_0)\rangle\langle\Psi(t_0)|$ as a minimum uncertainty coherent state, in which the degrees of freedom in the system are uncorrelated. More explicitly, we reprsent the pure state wavefunction Ψ at the initial time in the coordinate space representation as a separable product of all the modes:

$$\Psi(\mathbf{q}, t_0; \mathbf{\Gamma}_0) = \prod_k \Psi_k(q_k, t_0; p_{0k}, q_{0k}) \tag{10}$$

where k is the index for mode k, and the wavefunction for each mode has the form

$$\Psi_k(q_k, t_0; p_{0k}, q_{0k}) = (2\pi\sigma_{qk}^2)^{-1/4} \exp\left[-\frac{(q_k - q_{0k})^2}{4\sigma_{qk}^2} + ip_{0k}(q_k - q_{0k})\right] \tag{11}$$

In eq 11, σ_{qk}^2 represents the coordinate variance in the wavefunction Ψ_k and is related to its local harmonic frequency through the following relation:

$$\sigma_{qk}^2 = \hbar[4m\partial^2 V(\mathbf{q}_{0k})/\partial q_k^2]^{-1/2} \tag{12}$$

Furthermore, Ψ_k is a minimum uncertainty wave packet whose momentum spread is σ_{pk}, which is related to the coordinate spread through the uncertainty principle; $\sigma_{pk}^2\sigma_{qk}^2 = \hbar/2$. The wavefunction Ψ_k given by eq 11 corresponds to the initial dynamical component of the density matrix of the *kth* mode, ϱ_D^k, which can be expressed in the Wigner representation as

$$\varrho_D^k(p_k, q_k, t_0; p_{0k}, q_{0k}) = (2\pi\sigma_{pk}^2\sigma_{qk}^2)^{-1} \exp\left[-\frac{(p_k - p_{0k})^2}{2\sigma_{pk}^2} - \frac{(q_k - q_{0k})^2}{2\sigma_{qk}^2}\right] \tag{13}$$

We now consider the effective classical distribution $\rho_{cl}(p_0, q_0; T')$ associated with the initial dynamical component of the density matrix for each mode. We further enforce the constraint that each mode be associated with a single effective temperature T' at which the effective classical phase space distribution is constructed. In order to define the effective temperature T' uniquely, let us consider the case of a harmonic oscillator at temperature T, in which the exact density matrix at time t_0 is given by eq 7. The coordinate variance in $\rho_D^k(t_0)$ (eq 13) is given by $\sigma_{qk}^2 = \hbar/(2m\omega_k)$ (cf. eq 12), while the momentum variance is $\sigma_{pk}^2 = \hbar^2/(4\sigma_{qk}^2) = \hbar m\omega_k/2$, where ω_k is the vibrational frequency of the *kth* mode. Substituting eqs 7 and 13 into eq 5, we obtain the effective temperature

$$T'_k = \frac{\hbar\omega_k}{2k_B}\left[\coth\left(\frac{\hbar\omega_k}{2k_BT}\right) - 1\right] \tag{14}$$

Note that this effective temperature is smaller than T_c' (eq 8), the effective classical sampling temperature by an amount that is equal to the temperature associated with the zero-point energy. This is a reasonable result since the initial Gaussian wave packet associated with T' in eq 14 has taken the zero-point energy into account. The final formulation for the density matrix is given by the following equation:

$$\rho(\mathbf{q}, \mathbf{q}', t) = \int d\mathbf{\Gamma}_0\, \rho_{cl}(\mathbf{\Gamma}_0, T')\Psi(\mathbf{q}, t; \mathbf{\Gamma}_0)\Psi^*(\mathbf{q}', t; \mathbf{\Gamma}_0) \tag{15}$$

Here, we write both the final density matrix, ρ, on the left-hand side of eq 15, and the wavefunction Ψ in the coordinate space representation, with $\Psi(\mathbf{q},t; \mathbf{\Gamma}_0)$ being the wavefunction at time t with initial conditions given by eqs 10 and 11 at time t_0.

The exact time evolution of the Schrödinger wavefunction, $\Psi(\mathbf{q}, t; \mathbf{\Gamma}_0)$, can only be carried out for small dimensional systems. Many approximate approaches, such as the time dependent Hartree method,[52−54] have been devised for propagating the Schrödinger wavefunction in larger systems. In this paper, we approximate the temporal evolution of the Schrödinger wavefunction in Heller's Gaussian wave packet (GWP) picture as follows:[47]

$$\Psi(\mathbf{q},t; \mathbf{\Gamma}_0) = \exp\{(i/\hbar)[(\mathbf{q} - \mathbf{q}_t)^T\mathbf{A}_t(\mathbf{q} - \mathbf{q}_t) + \mathbf{p}_t(\mathbf{q} - \mathbf{q}_t) + \gamma_t]\} \tag{16}$$

We have already demonstrated previously that the semi-classical GWP approximation to the dynamics can be sufficiently accurate to solve the control equations on short time scales.[39] The wavefunction is assumed to remain Gaussian in functional form for all time, with the time dependence of the GWP being carried in the set of time dependent parameters $\{\mathbf{q}_t, \mathbf{p}_t, \mathbf{A}_t, \gamma_t\}$.[47] The time evolution of the full density matrix, ρ of eq 15, is then obtained by combining the semiclassical GWP dynamics with the initial classical phase space ensemble generated at the effective temperature T' given in eq 14.

Note that the semiclassical GWP approximation to the system dynamics is not essential to the approximate propagation scheme developed in this section, since we can incorporate more accurate quantum propagators to evolve the wavefunction. The key result here is that we have developed a novel working scheme which allows us to combine classical sampling techniques and quantum wavefunction dynamics to study both inhomogeneous structure effects and homogeneous dynamics effects in condensed phases. In the next section, we will apply the semiclassical approach developed in this section to quantum control in condensed phases.

III. Optimal Control in the Condensed Phase: Reduced-Density Matrix Formalism

The large dimensionality of the supersystem, aside from posing formidable computational difficulties, also poses basic questions with regard to quantum control. How should control be defined? How does the bath affect control? What can be controlled in a condensed-phase system that contains on the order of 10^{23} degrees of freedom? How will control degrade with time between the control pulses and the target time, the time at which we want the system to be controlled? How can we understand the degradation of control in systems with many degrees of freedom, for example, the difference between homogeneous and heterogeneous effects?

We take as our goal for control in a condensed-phase system the control of the small primary system only, leaving the bath degrees of freedom uncontrolled. In other words, the control object is the reduced density matrix of the supersystem defined in eq 4. The quantum control objective in this condensed-phase system is to find the light field $\epsilon(t)$ that best drives the reduced-density matrix to a selected target state at the target time t_f. For specificity, in all examples considered in this present work, the evolution of the reduced-density matrix on the excited state $|e\rangle$ will be controlled and the reduced-density matrix on the ground electronic state $|g\rangle$ is left uncontrolled. In this case, the target

operator has the following form:

$$\hat{A} = \hat{A}_e|e\rangle\langle e| \tag{17}$$

The objective is to maximize the target yield at the target time t_f in the reduced space, with the target yield given by the following:

$$A(t_f) = \mathrm{Tr}_{sys}[\hat{A}\rho^R(t_f)] = \mathrm{Tr}_{sys}[\hat{A}_e\rho_e^R(t_f)] \tag{18}$$

Here $\mathrm{Tr}_{sys}[...]$ denotes the trace over the degrees of freedom of the primary system, and $\rho_e^R(t)$ is the projection of the reduced-density matrix on the electronic excited state $|e\rangle$.

In the weak response regime, the density operator ρ_e^R is expanded in a perturbation series about the weak external field $\epsilon(t)$, keeping only the lowest nonvanishing term,

$$\rho_e^R(t) = (i/\hbar)^2 \int_{t_0}^{t} d\tau_2 \int_{t_0}^{\tau_2} d\tau_1\, E^*(\tau_2)E(\tau_1)\rho_e^0(t-\tau_2, \tau_2-\tau_1) + \mathrm{hc} \tag{19}$$

Here hc stands for the Hermitian conjugate of the first term; ρ_e^0 can be termed as the reduced bare density matrix since it is physically obtained from the density matrix created by a pair of separated delta (in time) pulses, and it is defined as

$$\rho_e^0(t_2,t_1) = (i/\hbar)^2\, \mathrm{Tr}_{bath}[G_{ee}(t_2)D_{ee,gg}G_{eg}(t_1)D_{eg,gg}\rho_g(-\infty)] \tag{20}$$

The reduced-density matrix written in eq 19 is what is created by the field $E(t)$ within first-order time-dependent perturbation theory. We also assume that the supersystem is initially prepared in a steady state (equilibrium, for example) on the electronic ground surface, i.e., $\rho(t_0) = \rho_g(t_0)|g\rangle\langle g|$, with $\rho_g(t_0) = \rho_g(-\infty)$. All the subscripts in the above formulas denote the electronic state. The quantities G_{uv} and $D_{uv,u'v'}$ are the elements of the total Green function and dipole operator, with the subscripts being labels such that $u, v = e$ or g denotes the matrix element with respect to electronic state.[34,55] In deriving eq 19, we have invoked the rotating wave approximation (RWA),

$$\epsilon(t) = E(t)e^{-i\omega_{eg}t} + E^*(t)e^{i\omega_{eg}t} \tag{21}$$

Here $E(t)$ is a complex, slowly varying field that is related to the completely real field $\epsilon(t)$ through the above equation. We determine the optimal field variationally subject to only a single constraint, this being that the total incident energy of the electric field in the time interval, $t_0 \le \tau \le t_f$, be fixed. This variational procedure leads to the following equation for the optimal control field $E(t)$,[10,33]

$$\int_{t_0}^{t_f} d\tau'\, M_s^R(\tau,\tau')E(\tau') = \lambda E(\tau) \tag{22}$$

In the above, $M_s^R(\tau,\tau')$ is termed the reduced material response function and is defined as

$$M_s^R(\tau,\tau') = [M_e^R(\tau',\tau)]^* \equiv M_e^R(t_f-\tau,\tau-\tau'), \quad \tau \ge \tau' \tag{23}$$

with

$$M_e^R(t_2,t_1) = \mathrm{Tr}_{sys}[\hat{A}_e\rho_e^0(t_2,t_1)] \tag{24}$$

The eigenvector corresponding to the largest eigenvalue λ is the globally optimal field in the weak response regime. A very similar integral equation for the control field has been derived previously when we had considered control of the full density matrix.[33] The control equations for the full density matrix and the reduced density matrix both have the same integral equation form, the only difference being that the kernel for control of the reduced-density matrix is the reduced material response function $M_s^R(\tau,\tau')$.

In the following, we will apply the semiclassical approach developed in the last section to evaluate both the reduced kernel, $M_e^R(t_2,t_1)$ in eq 24, and the second-order reduced density matrix, $\rho_e^R(t)$ in eq 19. The key component of these two quantities is the reduced bare density matrix ρ_e^0 in eq 20.

We now turn to the reduced bare density matrix $\rho_e^0(t_2,t_1)$ in eq 20. In the semiclassical picture (cf. eq 15), we may represent the reduced bare density matrix as

$$\rho_e^0(t_2,t_1) = \int d\mathbf{\Gamma}_0\, \rho_{cl}(\mathbf{\Gamma}_0;T')\rho_D^0(t_2,t_1;\mathbf{\Gamma}_0) \tag{25}$$

Here, $\rho_D^0(t_2,t_1;\mathbf{\Gamma}_0)$ is the reduced bare dynamical component of the density matrix, which depends only on the system degrees of freedom and defined as ($t_0 \to -\infty$)

$$\rho_D^0(t_2,t_1;\mathbf{\Gamma}_0) = \mathrm{Tr}_{bath}[(i/\hbar)^2 G_{ee}(t_2)D_{ee,eg}G_{eg}(t_1)D_{eg,gg}|\Psi_g(t_0;\mathbf{\Gamma}_0)\rangle\langle\Psi_g(t_0;\mathbf{\Gamma}_0)|] \tag{26}$$

$\Psi_g(t_0;\mathbf{\Gamma}_0)$, defined in the last section, is the initial wavefunction of the supersystem (system plus bath) on the ground electron state.

The final formulas for the reduced density matrix ρ_e^R (eq 19) and the reduced control response function M_e^R (eq 24) in the semiclassical picture are then (cf. eq 5) given by

$$\rho_e^R(t) = \int d\mathbf{\Gamma}_0\, \rho_{cl}(\mathbf{\Gamma}_0;T')\rho_D^R(t,\mathbf{\Gamma}_0) \tag{27}$$

$$M_e^R(t_2,t_1) = \int d\mathbf{\Gamma}_0\, \rho_{cl}(\mathbf{\Gamma}_0;T')M_D^R(t_2,t_1;\mathbf{\Gamma}_0) \tag{28}$$

In these equations, M_D^R and ρ_D^R are directly obtained by substituting eq 25 into eq 24 and eqs 25 and 26 into eq 19, respectively,

$$\rho_D^R(t,\mathbf{\Gamma}_0) = \int_{t_0}^{t}\int_{t_0}^{t} d\tau_2\, d\tau_1\, E^*(\tau_2)E(\tau_1)\rho_D^0(t-\tau_2, \tau_2-\tau_1;\mathbf{\Gamma}_0) \tag{29}$$

$$M_D^R(t_2,t_1) = \mathrm{Tr}_{sys}[\hat{A}_e\rho_D^0(t_2,t_1;\mathbf{\Gamma}_0)] \tag{30}$$

Equations 26−30 contain the main results of this section. Together with the semiclassical approach presented in the last section, these results provide a complete numerical procedure for evaluating the reduced density matrix, the reduced control response function, and the optimal control field.

As we have shown, the key quantity for the approximate temporal evolution of the reduced density matrix is the reduced bare dynamical component of the density matrix, ρ_D^0 in eq 26. We now present explicit coordinate and Wigner phase space representations of this quantity. In the coordinate representation, ρ_D^0 is given by (cf. eq 26)

$$\rho_D^0(\mathbf{Q},\mathbf{Q}',t_2,t_1;\mathbf{\Gamma}_0) = \int d\mathbf{x}\, \Psi_e^0(\mathbf{Q},\mathbf{x},t_2+t_1;\mathbf{\Gamma}_0)[\Psi_e^0(\mathbf{Q}',\mathbf{x},t_2;\mathbf{\Gamma}_0)]^* \tag{31}$$

The corresponding Wigner representation is then obtained via the Wigner transformation:

$$\rho_D^0(\mathbf{P}, \mathbf{Q}, t_2, t_1; \mathbf{\Gamma}_0) = (2\pi\hbar)^N \int_{-\infty}^{\infty} d\mathbf{s}\, e^{-iPs/\hbar} \rho_D^0(\mathbf{Q} + \mathbf{s}/2, \mathbf{Q} - \mathbf{s}/2, t_2, t_1; \mathbf{\Gamma}_0) \quad (32)$$

Here, N is the number of degrees of freedom in the supersystem. Note that after taking the trace over all bath modes **x** (i.e., the integration in eq 31), the above system density matrix can no longer be represented as a pure state. This is generally true in condensed-phase systems. Usually, the multidimensional integration over the bath modes **x** is an intractable task. However, in the GWP picture, since the wavepacket Ψ_e^0 is a Gaussian function in btoh the few primary system modes **Q** and the greater number of bath modes **x**, an analytical evaluation of the multidimensional Gaussian integration over all the bath modes **x** is possible. The reduced control response function can then be evaluated in the system coordinate representation via

$$M_e^R(t_2,t_1) = \int d\mathbf{\Gamma}_0\, \rho_{cl}(\mathbf{\Gamma}_0; T')[\int\int d\mathbf{Q}\, d\mathbf{Q}'\, A(\mathbf{Q}', \mathbf{Q})\rho_D^0(\mathbf{Q}, \mathbf{Q}', t_2, t_1; \mathbf{\Gamma}_0)] \quad (33)$$

or by the phase space representation via

$$M_e^R(t_2,t_1) = \int d\mathbf{\Gamma}_0\, \rho_{cl}(\mathbf{\Gamma}_0; T')[\int\int d\mathbf{P}\, d\mathbf{Q}\, A(\mathbf{P},Q)\rho_W^0(\mathbf{P}, \mathbf{Q}, t_2, t_1; \mathbf{\Gamma}_0)] \quad (34)$$

In next section, we will carry out a numerical simulation of a model system, I_2 in a low-temperature argon matrix.

IV. Control of I_2 in Ar: Simulation

A. Simulation Details. We now consider the condensed-phase model of I_2 in solid argon used in this work. Since the unit cell of the argon crystal is face centered cubic, we put 500 argon atoms[44,46,56−60] in a box with periodic boundary conditions. The system is allowed to equilibrate at 15 K and then the I_2 molecule is substituted for two adjacent argon atoms. The interaction potential between any two argon atoms and between any argon and iodine atom is modeled by a pairwise Leonard-Jones potential

$$V_{L\text{-}J}(r) = 4\epsilon((\sigma/r)^{12} - (\sigma/r)^6) \quad (35)$$

The potential parameters used in this work are tabulated in Table 1.[44,46,56−60] The potential for the I_2 excited A state is modeled by the following Morse potential:

$$V_A(R) = D_e(1 - e^{-\beta(R-R_e)})^2 \quad (36)$$

with the Morse potential parameters D_e, β, and R_e tabulated in Table 1. The potential for the I_2 X state is modeled by an RKR potential, which is tabulated elsewhere.[41]

In Figure 1 we show a schematic of the I_2 potential energy surfaces used in the calculations. The ground state is the $X(^1\Sigma^+)$ state and the excited state is the $A(^3\Pi_{1u})$ state. The lower arrow in Figure 1 indicates an electronic transition in the Frank−Condon region from the X to A state. As indicated by Figure 1, the gas-phase $X \rightarrow A$ transition at the photon energy shown is purely dissociative. This is niot the case when I_2 is embedded in the argon matrix, due to the caging of the I_2 by the surrounding argon atoms.[44−46] The probe state is the β state which, due to efficient solvent-induced electronic conversion,

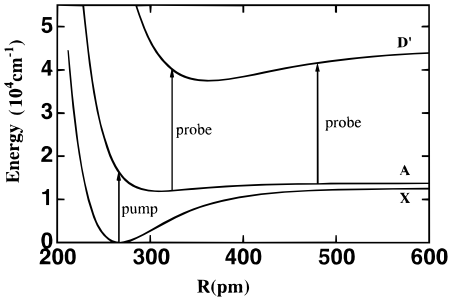

Figure 1. Schematic of the relevant I_2 potential energy surfaces, with the ion pair β and D′ states adjusted downward in energy by 2900 cm^{-1} to reflect the solvation by the Ar matrix. The vertical arrow from the ground X state to the excited A state shows the Frank−Condon transition, which is clearly unbound in the gas phase. The two vertical arrows from the A state to the β state indicate the two resonance windows that are opened in the pump−probe experiment. The internuclear distances R are expressed in picometers.

TABLE 1: Potential Parameters

potential parameters	values
D_e(A state)	1840 cm^{-1}
r_e(A state)	310 pm
β(A state)	2.147×10^{-2} pm^{-1}
ϵ_{Ar-Ar}	83.26 cm^{-1}
σ_{Ar-Ar}	340.5 pm
ϵ_{Ar-I}	130.24 cm^{-1}
σ_{Ar-I}	361.7 pm

relaxes to the D′ state. It is the D′ state that fluoresces, leading to the LIF signal.[44,45] In the condensed phase, these ion-pair states of I_2 are observed experimentally to be lowered in energy due to solvation. The lowering of the iodine β state reaches a limiting value of 4200 cm^{-1} for large I_2-Ar_n clusters ($n \geq 40$).[61−64] In argon matrices, the iodine D′ state is lowered by ∼2900 cm^{-1} [65] and is thus shown in Figure 1 as lowered by 2900 cm^{-1} from that of the gas phase along with the β state.

We now find the set of effective temperatures for the supersystem, which is at a temperature of 15 K. The ground-state vibrational frequency of molecular iodine is 214 cm^{-1}; therefore the effective temperature T' as defined by eq 14 is 3×10^{-7} K. For this initial calculation, we take the approximation of using the Debye frequency of the Ar matrix of 60 cm^{-1} as the single frequency of all the Ar atoms in the ground state; this sets the effective temperature T' at 2 K. Both of these effective temperatures are extremely small, and thus we can make the approximation that only a single initial configuration is needed, this being the configuration that is consistent with zero temperature; i.e., we only propagate a single pure state.

We now consider the exact flavor of GWP propagation that is to be used in the calculation (cf. see eq 16). We write the expansion of the potential energy function for the field-free Hamiltonian H_m in eq 2 as

$$V(Q, \mathbf{x}) = V_0(Q_t, \mathbf{x}_t) + \frac{\partial V}{\partial Q}[Q - Q_t] + \sum_k \frac{\partial V}{\partial x_k}[x_k - x_{k,t}] + \frac{1}{2}\frac{\partial^2 V}{\partial^2 Q}[Q - Q_t]^2 + \frac{1}{2}\sum_k \frac{\partial^2 V}{\partial^2 x_k}[x_k - x_{k,t}]^2 \quad (37)$$

where all derivatives are evaluated at the point (Q_t, $\mathbf{x}_t$). Here we omit the cross terms which couple the degrees of freedom, i.e., $[Q - Q_t]\sum_k[\partial^2 V/(\partial Q \partial x_k)][x_k - x_{k,t}]$. Within this approximation, the Schrödinger wave packet for the supersystem given in eq 16 remains in the following factorized form for all time:

$$\Psi(\mathbf{q},t) = \psi_Q(Q,t)\prod_k \psi_k(x_k,t) \quad (38)$$

The cross terms in the Taylor expansion are purposely neglected in order to enable the wave packet to be written in this factorized form, which both is much easier to propagate and enables the multidimensional integration needed to calculate the reduced material response function in eq 33 to be written as a simple product of single dimensional integrations. Although the neglect of the cross terms in the Taylor expansion of the potential is an approximation that was made for computational expediency, we believe that such an approximation is reasonable for the system of interest. The equations of motion for the phase space centers of the wave packet for the supersystem, ($\mathbf{q}_t$, $\mathbf{p}_t$), follow the fully coupled classical Hamilton equations. In other words, neglect of the correlation between the degrees of freedom in the wave packet does not mean that the guiding classical trajectories of the phase space centers of the wave packet are uncoupled. Since the second derivatives of the potential [evaluated at the point (Q_t, $\mathbf{x}_t$)] are time-dependent, the width parameters for each wave packet in eq 38 vary with time.

B. Results

To test our potentials and semiclassical quantum dynamics, before proceeding to a numerical study of quantum control on this system, we first consider a comparison of our semi-classical quantum dynamics simulation to the experimental pump−probe results obtained by Zadoyan and Apkarian.[44−46] We simulate the collected laser-induced fluorescence (LIF) signal that is obtained from their time-resolved pump−probe experiment using the classical Franck approximation[66]

$$S(t_d) \approx \int_{-\infty}^{\infty} dt\ \mathrm{Tr}[|\mu_{ef}(R)|^2 I_T(U_{fe},t)\rho_e(t+t_d)] \quad (39)$$

where $I_T(U_{fe}, t)$ is defined as

$$I_T(U_{fe}, t) = 2\ \mathrm{Re}\ E_T^*(t) \int_0^{\infty} dt'\ e^{i(U_{fe}-\Omega_T)t'} E_T(t+t') \quad (40)$$

and U_{fe} is defined as $U_{fe} = (V_f - V_e)/\hbar$, with V_f and V_e being the final probe state and excited-state potential energy surfaces, respectively. Here Ω_T is the carrier frequency of the probe field, $\mu_{ef}(R)$ is the transition dipole between the excited and final probe states, with R being the I_2 internuclear distance, and $\rho_e(t)$ is the system excited electronic state density matrix. In the absence of global information about the final probe state potentials energy surface in the condensed phase, we further assume that only the resonance windows contribute to the collected LIF signal. The resonance windows are roughly estimated by lowering the gas-phase ion-pair potential energy surface by 2900 cm^{-1}, as mentioned above.[61] Corresponding to the experimental conditions of Zadoyan and Apkarian,[44−46] we take the carrier wavelengths of the pump and probe fields to be 705 and 352.5 nm, respectively. With these assumptions, the carrier frequency of the probe pulse opens two resonance windows, one at $R =$ 320 pm and the other at $R = 480$ pm. These two probe windows are indicated in Figure 1 by the upper two vertical arrows that are drawn between the A state and the β state. Since these two windows are far apart, the value of the transition dipole moment may be different for each window. We estimate the dependence of the $\beta \leftarrow$ A transition dipole on internuclear I_2 distance by the following empirical formula for the D $\rightarrow$ X transition obtained from gas-phase experimental data[67]

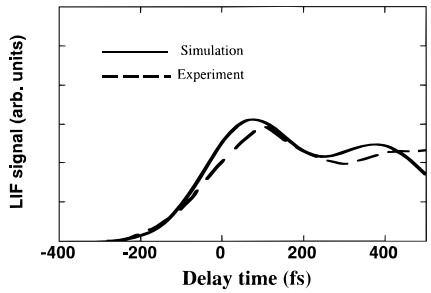

Figure 2. Collected LIF signal as a function of delay time between the centers of the pump and probe pulses for the experimental conditions of Zadoyan and Apkarian. The pump wavelength is 705 nm and probe wavelength is 352.5 nm. The dashed line is the experimental data and the solid line is the simulated signal.

$$\mu_{ef} = \frac{62.2}{R^2}\frac{1}{1+(R-4.1)^2} \quad (41)$$

Here the internuclear distance R is given in Å and μ_{ef} is given in debyes. As expected, the transition dipole for the valence to ion pair transition is smaller at larger internuclear distance R due to the difficulty of charge transfer. Although these data are for the transition D $\rightarrow$ X, rather than for the $\beta \leftarrow$ A transition considered in this work, and the data are for the gas phase rather than the condensed phase, lacking any other information above the coordinate dependence of the dipole transition moment we will use the above equation in this work. Based on this, we take the ratio of the transition dipole between the inner and outer windows to be $\mu_{in}/\mu_{out} \approx 2$. We take both the pump field and probe fields to be 106 fs intensity full width at half-height transform limited Gaussian pulses, yielding the value of 150 fs for the cross correlation that was measured under the experimental conditions of Zadoyan and Apkarian.[44−46] In Figure 2 we show the comparison of the simulated and experimental LIF signals as a function of delay time between the peak of the pump and probe pulses, up to a time delay of 500 fs. The dashed line is the experimental data and the solid line is the calculated LIF signal. The simulated and measured signals agree quite well up to this delay time. Degradation of accuracy in the calculated LIF signal at later times is to be expected, since the accuracy of GWP dynamics decreases as a function of time, because the underlying wave packets are forced to remain Gaussian, while real wave packets lose their simple shape in an anharmonic potential. Indeed the agreement between the experimental and simulated signal falls off after 500 fs. Thus we will try to control the dynamics of the system on a time scale that is less than 400 fs, where the agreement between the experiment and calculation is still quite good.

The control objective on the A state of I_2 chosen in this work is a cannon, i.e., a minimum uncertainty wave packet that has a positive value of momentum, meaning that the iodine atoms are moving away from each other. The functional form of this target in the Wigner representation is[34]

$$A_W(P,Q) = \frac{1}{\pi\hbar}\exp\Big(-\frac{2}{\hbar^2}[w_{QQ}(P-\bar{P})^2 + w_{PP}(Q-\bar{Q})^2 - 2w_{PQ}(P-\bar{P})(Q-\bar{Q})]\Big) \quad (42)$$

with $(w_{PP}w_{QQ} - w_{PQ}^2)^{1/2} = \hbar/2$ and with the phase space center of the target distribution given by ($\bar{Q}$, $\bar{P}$).

For the first case considered, we chose the cannon target parameters as $\bar{Q} = 380$ pm, $\bar{P}$ is chosen such that the kinetic energy is 2420 cm^{-1}, $\omega_{QQ} = \hbar/(2m\omega)$, $\omega_{PP} = m\omega\hbar/2$, and $\omega_{PQ} = 0$, with $\omega = 250$ cm^{-1}. The solid line in Figure 3 shows the

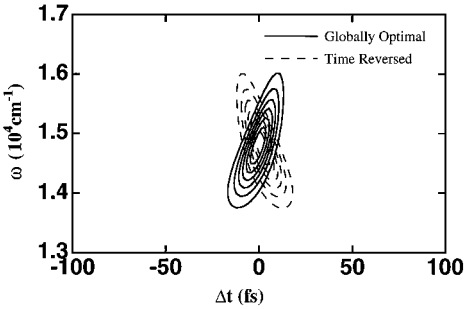

Figure 3. Wigner, representation of the globally optimal control field for the condensed-phase cannon target, solid line, and its time-reversal, dashed line. Δt is measured with respect to the temporal center of the pulses.

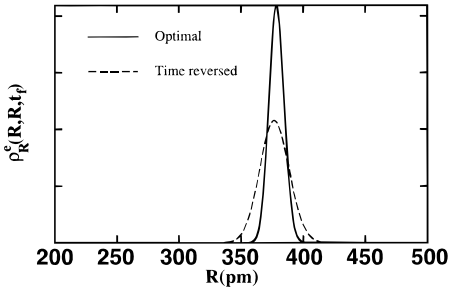

Figure 4. On-diagonal reduced density matrix created with the globally optimal field, solid line, and created with a time-reversed globally optimal field, dashed line. These give the probability distribution for the I_2 internuclear distance, independent of the Ar atoms.

Wigner transform of the computed globally weak response optimal field for this cannon target. Note that, for clarity, we used a window function in the plotting of the Wigner transform which reduces the interference normally present in the standard Wigner transform.[34,68,69] The globally optimal weak response field is a short pulse with an overall positive linear chirp, as expected from previous calculations.[34] Note that the time axis is labeled by Δt, which measures time from the temporal center of the globally optimal field.

We now calculate how well this globally optimal field has done with respect to reaching the desired objective. We term this measure the achievement and define the achievement as

$$\alpha(t_f) = \left(\frac{\mathrm{Tr}_{sys}[\hat{A}\rho_e^{\mathrm{R}}(t_f)]}{\mathrm{Tr}[\hat{A}]\ \mathrm{Tr}[\rho_e(t_f)]} \right)^{1/2} \tag{43}$$

Here $\rho_e^{\mathrm{R}}(t_f)$ is the field-initiated reduced density matrix created on the A state by the control field, which is given within first order time-dependent perturbation theory by eq 19. The achievement is designed to range between zero (no control) and unity (perfect control). The globally optimal field for the condensed-phase cannon target shown in Figure 3 leads to an achievement value of $\alpha = 0.89$. Calculations for such targets in the gas phase typically lead to values of the achievement on the order of 0.90−0.95, indicating that the ability to control the dynamics is somewhat hindered by the condensed-phase environment. This decrease in controllability in condensed-phase environments has been observed previously in our other theoretical calculations,[8,36,37] and even in a single oscillator bath,[70] and will be further discussed below.

Thus far the simulations have shown that there is partial controllability of the reduced density matrix in the condensed-phase system. We now turn to another more subtle question: is the control described above truly a coherent phenomena, in the sense that the control cannot be entirely explained just as a result of the frequency spectrum (intensity versus frequency) or just as a result of the intensity versus time of the pulse? In other words, must one include a higher order of description like "how does the frequency of the pulse vary with time" in order to explain its effect? In previous work on gas-phase I_2, we were able to answer this question in a positive way using the following argument. Take the time-reversal of the globally optimal field, shown as the dashed line in Figure 3, find the wave packet that is created by this time-reversed field, and compare this wave packet to the wave packet that is created by the globally optimal field. Since the time-reversed field and the original globally optimal field have identical frequency (i.e., power) spectra, $|E(\omega)|^2$, and very similar intensity versus time, $|E(t)|^2$, as can be seen from inspection of Figure 3 (with the knowledge that $|E(t)|^2$ is the projection of such a Wigner transform onto the time axis and similarly for $|E(\omega)|^2$ on the frequency axis), if the control were just a function of $|E(\omega)|^2$ and $|E(t)|^2$, the globally optimal field pulse and its time reversal should produce close to identical results on the wave packet. We now apply this test of coherent control for the cannon target in the condensed phase. In Figure 4, the solid line shows the on-diagonal reduced density matrix (the reduced density matrix equivalent of the pure state $|\Psi(R)|^2$, i.e., the probability density distribution for the I_2 internuclear distance irregardless of Ar atomic positions) that is created with the globally optimal cannon field and the dashed line that which is created by the time-reversal of the globally optimal cannon field. As indicated in Figure 4, the distribution created by the optimal field is much more focused than that created by the time-reversal of the globally optimal field. The achievement for the time-reversed globally optimal field in the condensed phase is $\alpha = 0.71$, to be contrasted with the achievement for the globally optimal field, $\alpha = 0.89$. The larger focusing and achievement for the globally optimal field than that for its time-reversal indicates that $|E(t)|^2$ and $|E(\omega)|^2$ cannot explain the control and that higher order coherent effects must be involved in reaching the target objective. We can approximately quantify this by defining the following "sophistication index",

$$\xi \equiv \alpha_{optimal} - \alpha_{time\text{-}reversed} \tag{44}$$

where $\alpha_{optimal}$ is the achievement for the globally optimal field and $\alpha_{time\text{-}reversed}$ is the achievement for the time-reverse of the globally optimal field. ξ is a measure of the sophistication of the field tailoring included in the control. The parameter ξ ranges from zero, if there is no sophistication as measured by the difference in achievement if the optimal field and its time reversal (for example, if the globally optimal control pulse is a transform limited pulse), to unity if a globally optimal field yields an achievement of unity while its time-reversal leads to an achievement of zero. A nonzero value of ξ indicates that the sophistication of the light pulse is playing a role in reaching the target objective. The value of ξ for the cannon target in the condensed phase is $\xi = 0.18$, indicating that there is a substantial component of sophistication involved in the control field, in that it and its time-reversal provide significantly different results as shown in Figure 4.

We now more completely investigate how the condensed-phase environment effects both the achievement, α, and the sophistication index, ξ. To do this we choose targets at successively larger I_2 internuclear distances, where the effect of the argon bath on the quantum dynamics becomes progressively more pronounced. We find it useful to choose targets for this study in the following way: (i) run classical trajectories on the composite supersystem, (ii) pick a value of $\bar{Q}$ for the coordinate space center of the target, (iii) choose the conjugate

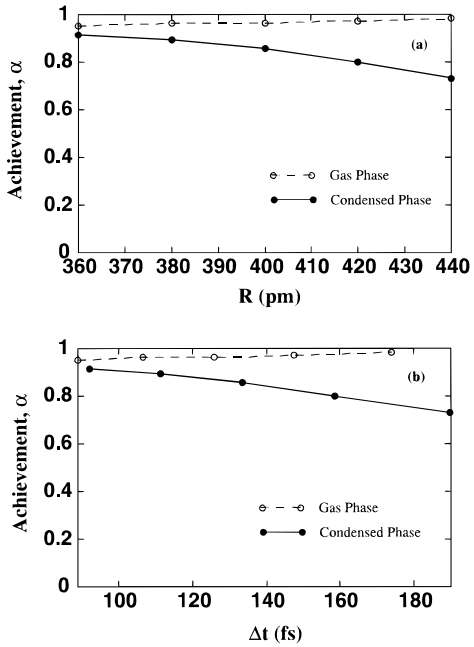

Figure 5. (a) The achievement, α, as a function of internuclear distance for the condensed-phase system, solid circles, and for the corresponding gas-phase system, open circles. (b) The achievement, α, as a function of Δt, the time between the peak of the optimal field and the target time, for the condensed-phase system, solid circles, and the gas-phase system, open circles.

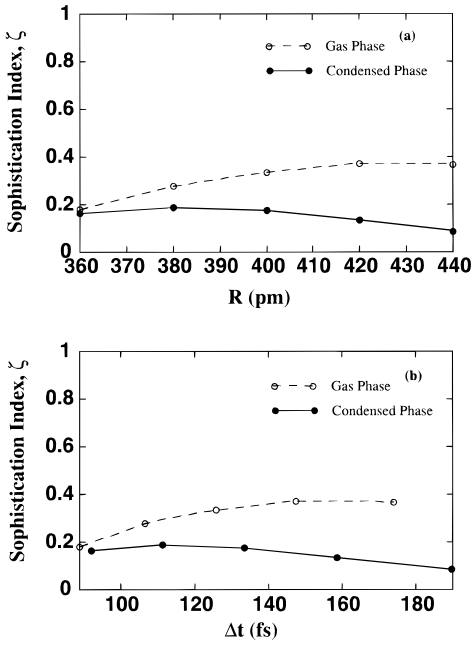

Figure 6. (a) The light field sophistication index, ζ, as a function of internuclear distance for the condensed-phase system, solid circles, and for the corresponding gas-phase system, open circles. (b) The sophistication index, ζ, as a function of Δt, the time between the peak of the optimal field and the target time, for the condensed-phase system, solid circles, and the gas-phase system, open circles.

value of the momentum along this trajectory as the value of the momentum center of the target, $\bar{P}$, and (iv) set the width of the minimum uncertainty target to be the same value $\omega_{QQ} = \hbar/(2m\omega)$ with $\omega = 250$ cm^{-1} for all internuclear distances. By choosing a series of targets in this way, we are assured that each target is achievable, since these targets have approximately the same expectation of the energy as that of the I_2 vibrational degree of freedom at any particular target internuclear position. To further demonstrate how the condensed-phase environment effects the controllability, we will compare the achievements and sophistication indices calculated for the condensed-phase system to their values in the corresponding gas-phase system. We also choose targets for the corresponding gas-phase system as outlined above, but using a gas-phase classical trajectory. This means that, for any given internuclear distance, the target for the gas phase and condensed phase will have the same width and the same coordinate space center but a different value for the momentum center. In Figure 5a, the solid circles show the achievement as a function of internuclear distance for the condensed phase, while the open circles show the achievement for the corresponding gas-phase system. It is evident that the achievement values are universally lower for the condensed-phase system than for the corresponding gas-phase system and that the achievement values for the condensed-phase system decrease as a function of increasing internuclear distance (and thus of time between control pulse and target), while the achievement values for the corresponding gas-phase system stay relatively constant as the internuclear distance of the target increases. In Figure 5b we show the achievement values as a function of Δt, the time between the peak of the optimal field and the target time. The open circles are the achievement values for the gas-phase system, and the solid circles are the achievement values for the condensed-phase system. These results demonstrate that the negative effect of the condensed-phase system on the controllability becomes more pronounced as the time and distance separating the initial controlling pulse and the ultimate target increase and the controlled I_2 chromophore interacts for a longer time and over a longer distance with the condensed-phase environment.

Now we consider the effect of the condensed-phase environment on the sophistication index ζ. In Figure 6a we show ζ as a function of internuclear distance for the condensed phase, solid circles, and for the gas phase, open circles. As indicated in Figure 6a, the value of ζ is universally lower in the condensed-phase system than in the corresponding gas-phase system. Also, the values for this parameter in general decrease as a function of internuclear distance for the condensed-phase system (and thus of time), while they monotonically increase in the gas-phase system. In Figure 6b we show the ζ values as a function of Δt. The open circles are the ζ values for the gas-phase system and the solid circles are the ζ values for the condensed-phase system. These results demonstrate that higher order coherence of the globally optimal field becomes less important in condensed-phase systems and that we have less ability as a function of time to control the reduced system by more sophisticated pulse tailoring techniques.

V. Conclusion

The present work has supported four major themes. The first is that a reasonable control objective in condensed phases is the reduced density matrix. The second is the development of a novel way to combine classical sampling techniques and quantum wave packet dynamics to study both inhomogeneous structure effects and homogeneous dynamic effects in condensed phases. The third is that semi-classical Gaussian wave packet (GWP) techniques coupled with approximate, nearly classical, nonzero temperature averaging procedures can lead to a tractable solution of the control equations in large quantum systems on short time scales. The fourth is that, although perfect coherent control is elusive, some degree of quantum control is still possible in a cold condensed phase quantum system on short time scales and that, on yet shorter time scales, more sophisticated pulse tailoring such as controlling the pulse chirp can be helpful.

It is not possible to control all 10^{23} degrees of freedom in a condensed phase quantum system. If, as is usually the case, there is a small subset of the composite system that one desires to control, the methodology we have presented here can be used for controlling this small subsystem. We reformulated quantum control in the weak response regime to control the reduced density matrix of the system. We have shown that the subsequent control equations for the reduced density matrix have a similar form to the control equations for the complete density matrix[33] and have presented a numerical algorithm for finding the optimal control fields once one knows the time-evolution of the system under the field-free Hamiltonian.

The solution of the multidimensional time-dependent Schrödinger equation (TDSE) must be used as input in order to determine the control fields for the reduced density matrix. In a condensed-phase system this input is impossible to compute exactly since, beyond a few dimensions, the multidimensional TDSE is impossible to solve exactly. Here we have employed an approximate solution scheme that seems to work, at least on the short time scale, that involves solving the TDSE with GWP dynamics. This approximation allows for a computationally tractable scheme for determining control fields on a short time scale.[39]

Numerically we have demonstrated that coherent quantum control is indeed possible in a cold, solid, condensed-phase system. We have shown that controllability, as expected, is degraded by the condensed-phase environment. These results are in parallel to work that we have done previously on I_2 that was immersed in a room temperature dense rare gas fluid[8,36,37] and to work on a molecule coupled to a one-dimensional bath.[70] In the work done on the liquid density system, it was found that coherent control is only possible at quite short times in the liquid density system. Here, we have found that sophisticated pulse tailoring can be useful in a cold solid-phase quantum system, more useful than in room temperature liquid density fluid, but not as useful as in the corresponding gas-phase system.

One major drawback to the work presented here is that we were forced to consider quantum control only on short time scales because the accuracy of our dynamical approximation scheme, i.e., GWP dynamics, is only reliable to about 400 fs in this system, since the GWP vibrational wave packet of the evolving I_2 is forced to remain Gaussian for all time. This limitation can be ameliorated by using the time-dependent Hartree (TDH) approximation, where the I_2 system vibrational wave packet is forced to remain factorized for all time but still retains the flexibility of allowing a full numerical grid calculation for the solution of the effective TDSE for each degree of freedom, so that the I_2 vibrational wave packet would not be forced to remain Gaussian. We have already shown in two dimensions that the TDH approximation can be quite accurate for the solution of the quantum control equations,[70] and it would be instructive to apply it to this condensed-phase case.

A drawback to the standard semi-classical GWP scheme for propagating the wavefunction is that it does not allow for the calculation of quantum control in the strong response regime, since it does not allow for the solution of a coupled two surface Hamiltonian, because the GWP is not allowed to bifurcate and thus be created on two potential energy surfaces simultaneously. Again, a way around this difficulty is to invoke the TDH approximation and treat the I_2 vibrational coordinate with a numerical grid.

While the application of quantum control to condensed-phase systems is still in a nascent stage, some patterns have already emerged from the work reported here combined with our earlier studies,[8,36,37,39,70] which can be considered as tentative conclusions to be further tested: (i) control can be achieved at short enough times between the controlling light field and target time but is less effective for the liquid and solid states than for the corresponding gas-phase cases and generally declines in effectiveness with increasing time and increasing distance of wave packet propagation, (ii) the average photon energy is, in general, greater for the same target than for the gas phase, to make up for the loss of energy to other degrees of freedom, and (iii) the sophistication of the optimal light fields is, in general, less than in the gas phase and declines further with increasing time and distance of wave packet propagation, as targets are set further away along a trajectory from the original atomic positions at the time of application of the control light field.

Acknowledgment. Y. Yan acknowledges support by the Honk Kong Government (RGC DAG94/95.SC05 and HKUST600/95P).

References and Notes

(1) Zewail, A. H. *Phys. Today* **1980**, *33*, 27.
(2) Tannor, D. J.; Rice, S. A. *Adv. Chem. Phys.* **1988**, *70*, 441.
(3) Manz, J., Parameter, C. S., Eds., Special Issue on Mode selectivity in Unimolecular Reactions. *Chem. Phys.* **1989**, *139* (1).
(4) Rice, S. A. *Science* **1992**, *258*, 412.
(5) Neuhauser, D.; Rabitz, H. *Acc. Chem. Res.* **1993**, *26*, 496.
(6) Warren, W. S.; Rabitz, H.; Dahleh, M. *Science* **1993**, *259*, 1581.
(7) Shapiro, M.; Brumer, P. *Int. Rev. Phys. Chem.* **1994**, *13*, 187.
(8) Krause, J. L.; Whitnell, R. M.; Wilson, K. R.; Yan, Y. J. In *Femtosecond Chemistry*; Manz, J., Wöste, L., Eds.; Springer-Verlag: Weinheim, 1995; p 743.
(9) Rice, S. A.; Zhao, M. In *Laser Techniques for State-Selected Chemistry II*; Hepburn, J. W., Ed.; SPIE: Bellingham, WA, 1994; Vol. 2124, p 246.
(10) Tannor, D. J.; Rice, S. A. *J. Chem. Phys.* **1985**, *83*, 5013.
(11) Shapiro, M.; Brumer, P. *J. Chem. Phys.* **1986**, *84*, 4103.
(12) Muller, H. G.; Bucksbaum, P. H.; Schumacher, D. W.; Zavriyev, A. *J. Phys. B* **1990**, *23*, 2761.
(13) Baranova, B. A.; Chudinov, A. N.; Zel'dovich, B. Y. *Opt. Commun.* **1990**, *79*, 116.
(14) Schafer, K. J.; Kulander, K. C. *Phys. Rev. A* **1992**, *45*, 8026.
(15) Shi, S. H.; Rabitz, H. *J. Chem. Phys.* **1990**, *92*, 2927.
(16) Weiner, A. M.; Leaird, D. E.; Wiederrecht, G. P.; Nelson, K. A. *Science* **1990**, *247*, 1317.
(17) Chelkowski, S.; Bandrauk, A.; Corkum, P. B. *Phys. Rev. Lett.* **1990**, *65*, 2355.
(18) Jakubetz, W.; Manz, J.; Schreier, H.-J. *Chem. Phys. Lett.* **1990**, *165*, 100.
(19) Janszky, J.; Adam, P.; Vinogradov, A. V.; Kobayashi, T. *Chem. Phys. Lett.* **1993**, *213*, 368.
(20) Dunn, T. J.; Sweetser, J. N.; Walmsley, I. A.; Radzewicz, C. *Phys. Rev. Lett.* **1993**, *70*, 3388.
(21) Kaluza, M.; Muckerman, J. T. *J. Chem. Phys.* **1995**, *102*, 3897.
(22) Judson, R. S.; Lehmann, K. K.; Rabitz, H.; Warren, W. S. *J. Mol. Struct.* **1990**, *223*, 425.
(23) Shapiro, M.; Brumer, P. *J. Chem. Phys.* **1991**, *95*, 8658.
(24) Cina, J. A.; Harris, R. A. *J. Chem. Phys.* **1994**, *100*, 2531.
(25) Melinger, J. S.; Hariharan, A.; Gandhi, S. R.; Warren, W. S. *J. Chem. Phys.* **1991**, *95*, 2210.
(26) Melinger, J. S.; Gandhi, S. R.; Hariharan, A.; Goswami, D.; Warren, W. S. *J. Chem. Phys.* **1994**, *101*, 6439.
(27) Chen, C.; Yin, Y. Y.; Elliott, D. S. *Phys. Rev. Lett.* **1990**, *64*, 507.
(28) Park, S. M.; Lu, S. P.; Gordon, R. J. *J. Chem. Phys.* **1991**, *94*, 8622.
(29) Sugawara, M.; Fujimura, Y. *J. Chem. Phys.* **1994**, *100*, 5646.
(30) Herek, J. L.; Materny, A.; Zewail, A. H. *Chem. Phys. Lett.* **1994**, *228*, 15.
(31) Zadoyan, R.; Apkarian, V. A. *Chem. Phys. Lett.* **1993**, *206*, 475.
(32) Krause, J. L.; Wilson, K. R.; Yan, Y. J. In *Laser Techniques for State-Selected Chemistry II*; Hepburn, J. W., Ed.; SPIE: Bellingham, WA, 1994; p 258.
(33) Yan, Y. J.; Gillilan, R. E.; Whitnell, R. M.; Wilson, K. R.; Mukamel, S. *J. Phys. Chem.* **1993**, *97*, 2320.
(34) Krause, J. L.; Whitnell, R. M.; Wilson, K. R.; Yan, Y. J.; Mukamel, S. *J. Chem. Phys.* **1993**, *99*, 6562.
(35) Kohler, B.; Krause, J. L.; Raksi, F.; Rose-Petruck, C.; Whitnell, R. M.; Wilson, K. R.; Yakovlev, V. V.; Yan, Y. J.; Mukamel, S. *J. Phys. Chem.* **1993**, *97*, 12602.
(36) Kohler, B.; Krause, J. L.; Raksi, F.; Rose-Petruck, C.; Whitnell, R. M.; Wilson, K. R.; Yakovlev, V. V.; Yan, Y. J. In *Reaction Dynamics*

in Clusters and Condensed Phases; Jortner, J., Levine, R. D., Pullman, B., Eds.; Kluwer: Dordrecht, 1994; pp 495−507.
(37) Krause, J. L.; Whitnell, R. M.; Wilson, K. R.; Yan, Y. J. In *Ultrafast Reaction Dynamics and Solvent Effects*; Gauduel, Y., Rossky, P., Eds.; American Institute of Physics: New York, 1994; p 3.
(38) Kohler, B.; Krause, J.; Raksi, F.; Wilson, K. R.; Whitnell, R. M.; Yakovlev, V. V.; Yan, Y. J. *Acc. Chem. Res.* **1995**, *28*, 133.
(39) Messina, M.; Wilson, K. R. *Chem. Phys. Lett.* **1995**, *241*, 502.
(40) Krause, J. L.; Messina, M.; Wilson, K. R.; Yan, Y. J. *J. Phys. Chem.*, in press.
(41) Che, J.; Krause, J. L.; Messina, M.; Wilson, K. R.; Yan, Y. J. *J. Phys. Chem.*, in press.
(42) Kohler, B.; Krause, J. L.; Whitnell, R. M.; Wilson, K. R.; Yakovlev, V. V.; Yan, Y. J. In *Ultrafast Phenomena IX*; Mourou, G. A., Zewail, A. H., Barbara, P. F., Knox, W. H., Eds.; Springer-Verlag: Berlin, 1994; p 44.
(43) Kohler, B.; Yakovlev, V. V.; Che, J.; Krause, J. L.; Messina, M.; Wilson, K. R.; Schwentner, N.; Whitnell, R. M.; Yan, Y. J. *Phys. Rev. Lett.* **1995**, *74*, 3360.
(44) Zadoyan, R.; Li, Z.; Ashjian, P.; Martens, C. C.; Apakarian, V. A. *Chem. Phys. Lett.* **1994**, *218*, 504.
(45) Zadoyan, R.; Li, Z.; Martens, C. C.; Apkarian, V. A. *J. Chem. Phys.* **1994**, *101*, 6648.
(46) Li, Z.; Zadoyan, R.; Apkarian, V. A.; Martens, C. C. *J. Phys. Chem.* **1995**, *99*, 7453.
(47) Heller, E. J. *J. Chem. Phys.* **1975**, *62*, 1544.
(48) Mukamel, S. In *The Principles of Nonlinear Optical Spectroscopy*; Oxford University Press: New York, 1995.
(49) Berman, M.; Kosloff, R. *Comput. Phys. Commun.* **1991**, *63*, 1.
(50) Yan, Y. J.; Mukamel, S. *J. Chem. Phys.* **1988**, *88*, 5735.
(51) Bergsma, J. P.; Berens, P. H.; Wilson, K. R.; Fredkin, D. R.; Heller, E. J. *J. Phys. Chem.* **1984**, *88*, 612.
(52) Dirac, P. A. M. *Proc. Cambridge Philos. Soc.* **1930**, *26*, 376.
(53) Frenkel, J. *Wave Mechanics*; Oxford University Press: Oxford, 1934.
(54) McLachlan, A. D. *Mol. Phys.* **1964**, *8*, 39.
(55) Fano, U. *Rev. Mod. Phys.* **1957**, *29*, 74.
(56) Fincham, D.; Heyes, D. M. *Adv. Chem. Phys.* **1985**, *63*, 493.
(57) Allen, M. P.; Tildesley, D. J. *Computer Simulation of Liquids*; Clarendon Press: Oxford, 1987.
(58) Hockney, R. W.; Eastwood, J. W. *Computer Simulation Using Particles*; McGraw-Hill Inc.: New York, 1981.
(59) Scoles, G. *Annu. Rev. Phys. Chem.* **1980**, *88*, 81.
(60) Ciccotti, G., Frenkel, D., McDonald, I. R., Eds. *Simulation of Liquids and Solids. Molecular Dynamics and Monte Carlo Methods in Statistical Mechanics*; North-Holland: Amsterdam, 1987.
(61) Wan, J. K.; Liu, Q.; Zewail, A. H. *J. Phys. Chem.* **1995**, *99*, 11309.
(62) Potter, E. D.; Liu, Q.; Zewail, A. H. *Chem. Phys. Lett.* **1992**, 605.
(63) Liu, Q.; Wang, J.-K.; Zewail, A. H. *Nature* **1993**, *364*, 427.
(64) Fei, S.; Zheng, X.; Heaven, M. C.; Tellinghuisen, J. *J. Chem. Phys.* **1992**, *97*, 6057.
(65) Macler, M.; Heaven, M. C. *Chem. Phys.* **1991**, *151*, 219.
(66) Lax, M. *J. Chem. Phys.* **1950**, *20*, 1752.
(67) Tellinghuisen, J. *Can. J. Phys.* **1984**, *62*, 1933.
(68) Kosloff, R.; Rice, S. A.; Gaspard, P.; Tersigni, S.; Tannor, D. J. *Chem. Phys.* **1989**, *139*, 201.
(69) Paye, J. *IEEE J. Quantum Electron.* **1992**, *28*, 2262.
(70) Messina, M.; Wilson, K. R.; Krause, J. L. *J. Chem. Phys.*, in press.

JP953059E